Cyclic High Pressure Torsion of Nickel and Armco Iron

Florian Wetscher, Reinhard Pippan

Cyclic High Pressure Torsion of Nickel and Armco Iron

Journal:	*Philosophical Magazine & Philosophical Magazine Letters*
Manuscript ID:	TPHM-05-Nov-0533.R1
Journal Selection:	Philosophical Magazine
Date Submitted by the Author:	16-Feb-2006
Complete List of Authors:	Wetscher, Florian; Erich Schmid Institute of Materials Science; CD-Laboratory for Local Analysis of Deformation and Fracture Pippan, Reinhard; Erich Schmid Institute of Materials Science; CD-Laboratory of Local Analysis of Deformation and Fracture
Keywords:	deformation, nanostructured materials, cyclic deformation
Keywords (user supplied):	high pressure torsion
Note: The following files were submitted by the author for peer review, but cannot be converted to PDF. You must view these files (e.g. movies) online.	
chptbib.bib	

Cyclic High Pressure Torsion of Nickel and Armco Iron

F. Wetscher[1,2,*] and R. Pippan[1,2]

[1]Erich Schmid Institute for Materials Science, Austrian Academy of Sciences, A-8700 Leoben, Austria

[2]CD-Laboratory for Local Analysis of Deformation and Fracture, Jahnstr. 12, A-8700 Leoben

Abstract

Cyclic high pressure torsion, **a modified version of high pressure torsion**, is applied to Armco-iron and nickel. The results in terms of microstructure and flow stress are compared to samples deformed by conventional high pressure torsion. For both processes and both materials, a saturation in the decrease of the structure size and the increase in the flow stress is observed. The minimum size of the structural elements which is obtainable is smallest for the conventionally high pressure torsion deformed samples and increases with decreasing strain per cycle in cyclic high pressure torsion.

*Corresponding author. Tel.: +43 3842 804 310; fax: +43 3842 804 116; e-mail: wetscher@unileoben.ac.at

1 Introduction

In the last years numerous papers have proven the capability of the methods of severe plastic deformation (SPD) to produce ultra fine grained and nanograined materials for new applications, see for example [1, 2, 3]. Especially by using equal channel angular pressing (ECAP) with the different routes it is possible to determine the influence of the strain path on grain refinement and the mechanical properties [4, 5]. Nevertheless, the possibilities to vary the strain per pass are very limited and do in most cases comprise a change in the geometry of the tool or the application of composed passes as used in [4]. Furthermore, the total strain reachable by ECAP is limited by practical considerations. The applying of extremely high strains is very time-consuming for the incremental process of ECAP. The simplest method to reach extremely high strains is high pressure torsion (HPT)[6, 7, 8], with the restriction that no change in the strain path can be achieved easily.

Therefore, in this paper a cyclic form of HPT is introduced, cyclic high pressure torsion (CHPT). Due to modifications of our HPT tool it is now possible to cyclically reverse the deformation after a chosen time. The aim of this study is to evaluate the differences between samples deformed by HPT and CHPT in terms of microstructure and mechanical strengths and the influence of the strain per cycle over a wide range of this value.

2 Experimental

The materials used in this study are the bcc Armco iron and the fcc nickel (99.99%). Disks of the materials with an original grain size of approximately $50\mu m$ were produced with a radius r of 4 mm and a thickness t of 0.8 mm. These disks were deformed by HPT to a total equivalent strain of 64 and CHTP to total equivalent shear strains $\epsilon_{eq,tot}$ of 4, 8, 32 and 64 at a radius $r = 3$ mm.

The shear strain per cycle $\Delta\epsilon$ was choosen to be 0.5, 1, 2 and 4 at a radius of $r = 3$ mm for this investigation. For comparision, samples of nickel with $\Delta\epsilon =$ 0.5 and 4 and $\epsilon_{eq,tot}$=256 were also examined. The total equivalent shear strain and the strain per cycle are calculated according to Eq. 1 and Eq. 2 where φ is the rotation angle and m is the number of cycles[†].

$$\Delta\epsilon_{eq} = \frac{\varphi r}{t\sqrt{3}} \tag{1}$$

$$\epsilon_{eq,tot} = m\Delta\epsilon_{eq} \tag{2}$$

The hydrostatic pressure was kept constant for all experiments at a value of 5.7 GPa, the number of turns per minute was 0.2. All deformation experiments were carried out at room temperature, no significant heating of the samples due to the deformation did occur. To evaluate the changes of the flow stress, the torque was measured in-situ by means of strain gauges. From this measured torque, an upper value for the flow stress can be calculated [9, 10]. A sketch of our HPT-tool can be seen in Figure 1. The microstructure was investigated with a Zeiss 1525 scanning electron microscope (SEM) at 20kV using backscattered electrons (BSE). Orientation image maps were measured for nickel samples deformed with a $\Delta\epsilon$ of 0.5 and 4 by analyzing the Kikuchi patterns caused by back scattered electrons (EBSD). The sample preparation comprised consecutive grinding, polishing, etching and a final polishing step. Special care was taken that the samples were not exposed to elevated temperatures during this process to prevent recrystallisation. All micrographs were taken in radial direction as can be seen in Fig. 2.

[†]one cycle means a deformation in one direction, similar to one pass in ECAP, it corresponds to $\frac{1}{2}$ cycle in conventional fatigue

3 Results

3.1 Flow stress

A typical measurement of the torque which can be related to the flow stress during CHPT with a $\Delta\epsilon = 1$ of Armco iron as a function of time which is proportional to the accumulated strain is presented in Figure 3a. The negative values of the *flow stress* correspond to an arbitrary definition of a positive and negative direction of the deformation. At the first few cycles, the increase of the flow stress would be almost identical to the flow curve of monotonic deformed samples when absolute values are taken. **In both materials a pronounced work hardening at the first few cycles is present, with an increasing number of cycles the increase of the absolute value of the maximum of the flow stress becomes very low. With higher total strains the cyclic flow curve shows another feature. After changing the strain path, the shear stress at the beginning of the new cycle is markedly lower as the maximum shear stress at the end of the previous cycle and a period with a slow increase of the flow stress is present.** As can be seen in Figure 3b for nickel, this behavior depends on the strain per cycle. It is most pronounced at $\Delta\epsilon = 1$ and 2. After this, a further work hardening occures with a steep increase of the flow stress until it reachs approximately the same absolute value at the end of the cycle as in the previous one. (Figure 4). It can be seen in Fig. 3b that the slope of this hardening stage decreases with increasing $\Delta\epsilon$. Figure 4a and 4b show the maximum of the flow stresses at each cycle as a function of the total deformation for all applied $\Delta\epsilon$ for Armco iron and nickel, respectively. In both materials the same features are visible. Just like in the monotonic deformed samples, the maximum torque saturates after a certain saturation strain. The lower the $\Delta\epsilon$ is, the lower is also the strain necesarry for the onset of this steady state deformation. The quickest saturation can be observed at a $\Delta\epsilon = 0.5$, the highest strain to reach the saturation is necessary

for the monotonic deformation. It can also be noted for both materials that the higher $\Delta\epsilon$ was, the closer are the curves to the curve for the monotonic deformed samples after the onset of saturation. A difference between the two materials is also the onset strain for the saturation. This strain is higher for the bcc iron compared to the fcc nickel. The maximum torque and therefore the maximum flow stress is slightly higher for Armco iron than for nickel.

3.2 Microstructure

The resulting microstructures after a deformation to a total strain of $\epsilon_{eq,tot} = 64$ for different $\Delta\epsilon$ as can be seen by using backscattered electrons are depicted in Fig. 5 and Fig. 6 for Armco iron and nickel. In all presented micrographs the baseline of the picture is parallel to the shear plane. For both materials the same features are recognizable. The microstructure for the samples with $\Delta\epsilon = 0.5$ consists of quite equiaxed elements, the structure size is markedly smaller than 1 μm, only a weak preferred direction of the elements is detectable. With increasing $\Delta\epsilon$ a decreasing structure size and an aspect ratio of the elements markedly larger than 1 can be observed. Furthermore, a preferred direction of the structural elements is now present. The microstructure of the nickel samples deformed monotonically and the sample deformed with $\Delta\epsilon = 4$ are almost identical. The alignment of the structural elements is naturally in the opposite direction, because the last cycle in the CHPT experiments is always in the 'negative' direction.

In Figure 7, the microstructure of Nickel after monotonic deformation to strains of ϵ_{eq}=0.5, 1, 2 and 4 (as large as the strain increments in the CHPT experiments) is depicted. After a strain of $\epsilon_{eq} = 0.5$ the beginning of the formation of a substructure within a grain can be seen. When the strain gets larger, more and more well defined elements form, until the whole microstructure is very homogeneous,

compare Figure 6e and Figure 7d. During further deformation, the microstructure is still somewhat refined, until this process reachs a steady state.

Figure 8 shows the inverse pole figures calculated from the EBSD measurements for different stages of the development of the microstructure for nickel samples deformed with $\Delta\epsilon = 0.5$ and $\Delta\epsilon = 4$. The white lines correspond to boundaries with a missorientation between 2°and 15°, the black lines show boundaries with a missorientation greater than 15°. It can be seen that after a deformation to total strains higher than 16 no significant changes in the structure size occurs. The differences between the samples deformed with $\Delta\epsilon = 0.5$ and $\Delta\epsilon = 4$ are similar to those seen in the BSE-micrographs.

The evolution of the structural size as well as the ratio of the length of high angle boundaries (HAB) ($\geq$15°) to low angel boundaries (LAB) (2°-15°) for nickel is presented in Figure 9. The grain size presented here was evaluated from the EBSD measurements using a missorientation of $\geq$ 5°as a criterion to define a grain boundary. Again, a saturation in the decrease of the structural size can be seen. With increasing total strain, the fraction of the high angle boundaries increases, somewhat faster for the samples with the higher $\Delta\epsilon$. It can be seen that the higher the $\Delta\epsilon$ was, the higher was the fraction of the HAG. The highest value for the fraction of the HAG as well as the smallest structure size was measured for the monotonic deformed sample.

In Fig. 10, the missorientation angle distributions of the nickel samples are compared to the random Mackenzie distribution. Only missorientations larger than 5°were taken into account for the calculation of these graphs. Of course, a lot of boundaries with smaller missorientations exists, but they are mainly within the grains. For the samples deformed with $\Delta\epsilon = 0.5$ almost no correlation between the missorientation distribution and the random distribution can be seen. For higher total deformations, a slightly higher amount of high angle boundaries is present, but the fraction of small missorientations is still

very high. In contradiction to this, the missorientation distribution of samples deformed with $\Delta\epsilon = 4$ converge to the random distribution with increasing total strain. The samples deformed up to $\epsilon_{eq,tot} = 256$ as well as the missorientation distribution of the monotonic deformed sample with $\epsilon_{eq} = 64$ show no further shift to higher missorientation angles.

4 Discussion

The cyclic high pressure torsion can be seen in two contexts. Firstly, as an advancement of the conventional high pressure torsion and also as a similar process like ECAP Route C, and secondly, as a borderline case of fatigue.

4.1 Severe Plastic Deformation

SPD of pure metals is quite common and therefore a number of papers deal with the evolution of the microstructure and mechanical properties of nickel and pure iron. After HPT, grain sizes in the range of 100 nm to 400nm for nickel are reported in the literature [11, 12, 13, 14]. The grain sizes reported for nickel after ECAP are quite higher, namely between 300nm and 450nm [14, 15, 16, 17]. When comparing such results, one has always to take care that different methods are used to evaluate the grain size. Another important factor is the level of impurities and alloying elements of the used materials [18]. Similar results are reported for SPD of pure iron [19, 20, 21]. In the present investigation, the structure size at saturation of nickel was determined from 370 nm for the monotonic deformed samples up to 850 nm for the samples deformed with $\Delta\epsilon = 0.5$.

The determination of the structure size as well as the measurement of the flow curve both for nickel and Armco-iron clearly show that in HPT experiments after a total equivalent strain larger than approximately 20 no further refinement of the structure occures. **This behavior was also shown for pure copper**

in HPT experiments[9, 22]. A similar saturation in the structure size and in the mechanical strength can also be observed in CHPT experiments, as can be seen in Figure 3 and Figure 8. It can be seen that the strain necessary for the onset of saturation depends on the strain increment $\Delta\epsilon$. The larger $\Delta\epsilon$ is, the larger has to be that onset strain and the more similar is the microstructure of CHPT deformed samples compared to the microstructure of monotonic HPT deformed samples. Hence, an obvious result is that the strain per cycle clearly determines the resulting structure size. Conventional HPT could be compared to ECAP Route A, where there is no rotation of the billet between the passes. Hence, elements are continiously sheared in one direction during multiple passes[23]. CHPT is more comparable to ECAP Route C, where the billet is rotated by 180°along the billet axis. This leads to a foreward and backward shearing of an element during successive passes[23]. Therefore, it can be concluded that ECAP Route A will be more effective than Route C in terms of grain refinement, although not necessarily in terms of producing an equiaxed microstructure. This behavior should be well pronounced in most ECAP processes, where a tool angle of 90°is used and the resulting strain per pass is equal to 1. But as can be seen in Fig. 4, the differences at the beginning are not so large as in the steady state regime. This effect of the strain path at ECAP was also found in other studies, for instance in [24, 25]. The conflictive results from other studies [26] may be contributed to the smaller differences at low total strains where the differences are not as significant.

In contrast to the saturation in grain size and the mechanical strength, it seems that the ratio between the length of the HAB and LAB as well as the increase in missorientation between neighbouring elements does not saturate as fast as the strength. Hence, one can assume that the mechanical strength is mainly determined by the size of the structural elements and not by the missorientation

between these elements.

Why does the structure size saturate in HPT and CHPT at different levels?

The saturation of the structure size in single phase materials due to severe plastic deformation and its reasons is a topic that is not widely discussed in the literature until recently [22, 27, 28]. It is assumed that processes similar to dynamic recrystallisation or grain boundary sliding are taking place. For a more detailed discussion of this, see [22, 27].

Richert et al.[29] reported that similare stages of deformation are observed in cyclic experiments as in experiments with monotonic deformation, although the accumulated strains have to be much higher. The reason for this are annihilation processes that are induced by the reversal of the shear strain. Stüwe[30] described this behaviour mathematical by an efficiency factor η. This factor η describes the efficiency to create new dislocations and store them in the structure. Only η times the shear strain increment contributes to the increase in dislocation density. There are two limiting cases for η. If $\eta = 0$, no further strain hardening can occure. All dislocations that are created during the deformation in one direction run backwards and recombine in the former sources during the reversal of the deformation or the number of generated dislocations is equal to the number of annihilated dislocations in one cycle. The other case is that for both directions new dislocations are generated and are stored in the microstructure, therefore η would be equal to 1. If this is true there should be no difference between the cyclic and the monotonic deformation. In Figure 3a it can be seen that this may be the case for the very first few cycles. After a certain number of cycles, the efficiency factor decreases, until after the onset of saturation η is obviously zero over an even number of cycles and no further work hardening occurs. Hence, in this description of the process, the efficiency factor η is itself a function of the total strain and also differs for different $\Delta\epsilon$. It is near one at low total strain and approachs zero as the number of cycles

increases. **This efficiency factor can be a useful tool to describe cyclic deformation modes, although it has to be noted that no structural model is combined with it at the moment.**

But the detailed measurement of the torque show that this description with η is only true when one just looks at the reached maximum values for the torque at the end of the cycle. During the deformation, the torque and therefore the flow stress developes in a different way as described in section 3.1. As can be seen in Fig. 3, after a reversal of the strain path, the torque at the beginning of the cycle is significantly lower than the reached maximum torque after the previous cycle and increases only slightly for a significant fraction of the whole cycle. **This region may be the consequence of dislocations running backwards toward their sources or newly generated dislocations that annihilate with dislocation present on the same slip plane but with different sign from the previous cycle. Following this, the flow stress increases with a rate that is decreasing with increasing $\Delta\epsilon$. This means that after the process of a reversal of dislocation movement or annihilation of dislocations is exhausted, new dislocations are created to further plastically deform the sample.** For samples with a larger structure size (at the beginning of deformation or small $\Delta\epsilon$) a high work harding capability exists, therefore the rate of work hardening is large. For the samples with a structure size near the minimum structure size, almost no work hardening capability is left, leading to a slow increase of the flow stress. From the measurement it can be assumed that the flow stress and the structure size of cyclically deformed samples would reach the level of the monotonic deformed samples if the deformation would be carried on monotonic. This behavior can be seen for both materials with the before mentioned difference in the onset of the steady state region.

4.2 Fatigue

Of course, it has to be emphazised that the results from CHPT and HPT cannot directly be compared to results from fatigue tests. Nevertheless, many features that are well known in fatigue have similarities with the behaviour of CHPT deformed materials.

Fatigue of nickel and Armco-iron was investigated in many studies, see for example [31, 32, 33, 34, 35]. The presented cyclic hardening curves in these studies show similar characteristics like the measured curves in the present investigation. After an intense hardening stage at the beginning, the stress amplitude saturates in strain-controlled experiments. It is commonly reported [34, 36, 37, 38, 39] that the saturation stress is a function of the plastic strain amplitude for symmetric tension-compression tests both for various single- and polycrystalline materials. The saturation stress increases with the plastic strain amplitude, in some cases a plateau region exists as can be seen in Fig. 11a (from [38]). A question which was not solved till now is: Exists a limit for the cyclic hardening and, if it exists, where is it?

Of course, this can not be easily investigated due to the limit of the plastic strain amplitude in a compression-tension experiment. In the present study, these limits do not exist, although it has to be minded that the deformation mode is different. The increase of the saturation stress (here in terms of the torque) is compared to the monotonic flow curve in Fig. 11b and 11c for Armco-iron and nickel, respectively. For both materials it is obvious that the saturation stress increases with the plastic strain amplitude but the slope of this increase decreases markedly. Finally, for a $\Delta\epsilon = 4$, the saturation stress has about reached the saturation stress for the monotonic deformation mode. The data from conventional fatigue tests would just cover the very left side of the diagrams.

The occurrence of a saturation of the stress in fatigue is generally explained

by the development of a dislocation network that allows for a further deformation without an increase in the dislocation density. The cell size of this dislocation network decreases with increasing plastic strain amplitude and leads therefore to a higher saturation stress according to the mesh-length theory of work hardening [40]. Davidson and Lankford [41] measured the subgrain size in low carbon steels as a function of the cyclic stress range and compared them with results from other studies. A main result is the decrease of the subgrain size with the increasing cyclic stress, the smallest subgrains where found for the monotonic deformation in a tensile test. This is in good agreement with the present results as can be seen in Fig. 9a. The higher the $\Delta\epsilon$ was, the smaller was the structure size in the saturation regime. The smallest structure size was measured for the monotonic deformed sample. The decrease of the structure size for HPT-deformed copper was investigated by Hebesberger et al. [22]. They observed a saturation in the decrease of the structure size at higher strains similar as in the presented experiments in Armco iron and nickel.

Another feature of conventional fatigue tests is the onset of the saturation in mechanical strength. Generally it is reported that saturation is reached earlyer in terms of the number of cycles for larger plastic strain amplitudes. **When for example the results from [39] are expressed in terms of the product of number of cycles for saturation and the plastic strain amplitude (a value comparable to the equivalent strain as calculated in our study), the same behavior for fatigue and CHPT is present: The higher the strain per cycle, the higher has to be the accumulated strain until saturation occurs.** The highest total strain to reach the saturation is needed for the monotonic deformation in HPT.

In fatigue experiments, the typical plastic strain amplitudes are quite low (in the order of 10^{-3}) compared to the plastic strains in ECAP Route C or this investigation. Nevertheless, the cell size is comparable or only somewhat larger than the structure size after SPD and the laws govering this size seem to

be similar. The same characteristics both in terms of structure size and strain hardening are present in both processes. But the much higher stresses that are measured for SPD-deformed materials and now also for the CHPT deformed nickel and Armco iron show that especially the boundaries cannot be directly compared to the structures in fatigued materials. One difference is of course the higher missorientation between the elements in the SPD-deformed materials. But as could be seen in Fig. 10 and Fig. 4, the flow stress is mainly influenced by the structure size and not by the missorientation. Another difference is the high hydrostatic pressure under which SPD takes place. It is assumed [42] that the vacancy concentration is extremely high in these conditions and these vacancies may influence the formation of the boundaries. The boundaries (which are no real grain boundaries) in SPD-deformed materials are sometimes referred as non-equilibrium grain boundaries [6] and seem therefore be a special feature of the very large plastic strains only reached by applying the methods of SPD.

5 Conclusions

- Cyclic High Pressure Torsion, a modified version of High Pressure Torsion has been introduced, which permits to easily study many parameters of cyclic severe plastic deformation. The method has been applied to Armco iron and nickel.
- Monoton deformation by HPT of both material results in a saturation of strain hardening. A similar saturation occures due to deformation by cyclic high pressure torsion, but the accumulated strain to reach saturation decreases with decreasing $\Delta\epsilon$.
- The steady state that is reached in terms of mechanical strength is also reached in structure size, the differences in the saturation strength is also reflected in differences of the structure size. The only value that still

changes somewhat is the missorientation distribution. The higher the total deformation, the more similar is the orientation distribution to the Mackenzie distribution.

- **The structure size strongly depends on the strain increment. The larger the strain increment is, the smaller gets the structure size after the onset of saturation. The smallest structure size was reached for the monotonic deformation by High Pressure Torsion.**

6 References

References

[1] Y. T. Zhu, T. G. Langdon, R. S. Mishra, S. L. Semiatin, M. J. Saran, and T. C. Lowe, editors. *Ultrafine Grained Materials II*. TMS Publications, Warrendale, Pennsylvania, 2002.

[2] Y. T. Zhu, T. G. Langdon, R. Z. Valiev, S. L. Semiatin, D. H. Shin, and T. C. Lowe, editors. *Ultrafine Grained Materials III*. TMS Publications, Warrendale, Pennsylvania, 2004.

[3] M. J. Zehetbauer and R. Z. Valiev, editors. *Nanomaterials by Severe Plastic Deformation*. J. Wiley, VCH Weinheim (Germany), 2002.

[4] A. Vinogradov, T. Ishida, K. Kitagawa, and V.I. Kopylov. *Acta Mater.*, 53:2181–2192, 2005.

[5] P. L. Sun, P. W. Kao, and C. P. Chang. In Y. T. Zhu, T. G. Langdon, R. S. Mishra, S. L. Semiatin, M. J. Saran, and T. C. Lowe, editors, *Ul-*

trafine Grained Materials II, pages 35–42. TMS Publications, Warrendale, Pennsylvania, 2002.

[6] R. Z. Valiev, R. K. Islamgaliev, and I. V. Alexandrov. *Progr. Mat. Sci.*, 45:103–189, 2000.

[7] T. Hebesberger, A. Vorhauer, H. P. Stüwe, and R. Pippan. In M. J. Zehetbauer and R. Z. Valiev, editors, *Nanomaterials by Severe Plastic Deformation*, pages 447–452. J. Wiley, VCH Weinheim (Germany), 2002.

[8] A. Vorhauer and R. Pippan. *Scripta Mater.*, 51:921–925, 2004.

[9] F. Wetscher, A. Vorhauer, and R. Pippan. *Mat. Sci. Eng. A*, in press, 2005.

[10] A. Vorhauer and R. Pippan. *submitted to Acta Mater.*

[11] R. K. Islamgaliev, F. Chmelik, and R. Kuzel. *Mater. Sci. Eng., A*, 237:43–51, 1997.

[12] F. Dalla Torre, P. Spätig, R. Schäublin, and M. Victoria. *Acta Mat*, 53:2337–2349, 2005.

[13] E. Schaffler and R. Pippan. *Mat. Sci. Eng.A*, 387-389:799–804, 2004.

[14] A. P. Zhilyaev, B.-K. Kim, J. A. Szpunar, M. D. Baró, and T. G. Langdon. *Mat. Sci. Eng.A*, 391:377–389, 2004.

[15] K. Neishi, Z. Horita, and T. G. Langdon. *Mat. Sci. Eng.A*, 325:54–58, 2002.

[16] N. Hansen, X. Huang, and D. A. Hughes. In Y. T. Zhu, T. G. Langdon, R. S. Mishra, S. L. Semiatin, M. J. Saran, and T. C. Lowe, editors, *Ultrafine Grained Materials II*, pages 35–42. TMS Publications, Warrendale, Pennsylvania, 2002.

[17] N. Krasilnikov, W. Lojkowski, Z. Pakiela, and R. Valiev. *Mat. Sci. Eng.A*, 397:330–337, 2005.

[18] R. Pippan, A. Vorhauer, F. Wetscher, M. Faleschini, M. Hafok, and I. Sabirov. *Mater. Sci. Forum*, 503-504:407–412, 2006.

[19] R. Z. Valiev, Yu. V. Ivanisenko, E. F. Rauch, and B. Baudelet. *Acta Mat.*, 44:4705–4712, 1996.

[20] Yu. Ivanisenko, A. V. Sergueeva, A. Minkow, R. Z. Valiev, and H.-J. Fecht. In M. J. Zehetbauer and R. Z. Valiev, editors, *Nanomaterials by Severe Plastic Deformation*, pages 453–458. J. Wiley, VCH Weinheim (Germany), 2002.

[21] Florian Wetscher, Andreas Vorhauer, Richard Stock, and Reinhard Pippan. *Materials Science and Engineering A*, 387-389:809–816, 2004.

[22] T. Hebesberger, H. P. Stüwe, A. Vorhauer, F. Wetscher, and R. Pippan. *Acta Mater.*, 53:393–402, 2005.

[23] M. Furukawa, Y. Iwahashi, Z. Horita, M. Nomoto, and T. G. Langdon. *Mater. Sci. Eng.A*, 257:328–332, 1998.

[24] A. Gholinia, P. B. Prangnell, and M. V. Markushev. *Acta Mater.*, 48:1115–1130, 2000.

[25] L. Dupuy and E. F. Rauch. *Mat. Sci. Eng.A*, 337:241–247, 2002.

[26] T. C. Lowe, Y. T. Zhu, S. I. Semjatin, and D. R. Berg. In T. C. Lowe and R. Z. Valiev, editors, *Investigations and Applications of SPD*, page 237. Kluwer Academic Publishers, Norwell, 2000.

[27] H. P. Stüwe. *Mater. Sci. Forum*, 503-504:175–178, 2006.

[28] K. Nakashima, M. Suzuki, Y. Futamura, T. Tsuchiyama, and S. Takaki. *Mater. Sci. Forum*, 503-504:627–632, 2006.

[29] M. Richert, H. P. Stüwe, M. J. Zehetbauer, J. Richert, R. Pippan, Ch. Motz, and E. Schafler. *Mater. Sci. Eng., A*, 355:180–185, 2003.

[30] H. P. Stüwe. In M. J. Zehetbauer and R. Z. Valiev, editors, *Nanomaterials by Severe Plastic Deformation*, pages 55–64. J. Wiley, VCH Weinheim (Germany), 2002.

[31] D.J. Morrison and V. Chopra. *Mater. Sci. Eng., A*, 177:29–42, 1994.

[32] P. Lukas and L. Kunz. *Mater. Sci. Eng., A*, 189:1–7, 1994.

[33] C. Buque, J. Bretschneider, A. Schwab, and C. Holste. *Mater. Sci. Eng., A*, 300:254–262, 2001.

[34] Y. El-Madhoun, A. Mohamed, and M. N. Bassim. *Mater. Sci. Eng., A*, 385:140–147, 2004.

[35] H. Haddou, M. Risbet, G. Marichal, and X. Feaugas. *Mater. Sci. Eng., A*, 379:102–111, 2004.

[36] H. Mughrabi. *Mat. Sci. Eng.*, 33:207–223, 1978.

[37] A. Giese, A. Styczynski, and Y. Estrin. *Mat. Sci. Eng.A*, 124:L11–L13, 1990.

[38] C. D. Liu, M. N. Bassim, and D. X. You. *Acta metall. mater.*, 42:3695–3704, 1994.

[39] Y. El-Madhoun, A. Mohamed, and M. N. Bassim. *Mat. Sci. Eng.A*, 359:220–227, 2003.

[40] D. Kuhlmann-Wilsdorf. *Metall. Trans.*, 1:3173–3179, 1970.

[41] D. L. Davidson and J. Lankford. *Int. J. Fracture*, 17:257–275, 1981.

[42] M. Zehetbauer, H. P. Stüwe, A. Vorhauer, E. Schafler, and J. Kohout. In M. J. Zehetbauer and R. Z. Valiev, editors, *Nanomaterials by Severe Plastic Deformation*, pages 435–446. J. Wiley, VCH Weinheim (Germany), 2002.

List of Figure Captions

Fig.1 Sketch of the HPT-tool

Fig.2 Sample preparation for microscopy

Fig.3 (a) Measured torque during CHPT experiment, Armco-iron, $\Delta\epsilon = 1$ and during a HPT experiment (b) Details of measured torque curves during CHPT of nickel at different $\Delta\epsilon$, the decrease in the torque after changing the shear direction (+ and -) is indicated.

Fig.4 Measured torque during HPT and the maximum torques in the CHPT experiments (a) for Armco-iron and (b) for nickel

Fig.5 SEM micrographs of Armco-iron taken in radial direction for $\epsilon_{eq,tot} = 64$ at (a) $\Delta\epsilon = 0.5$, (b)$\Delta\epsilon = 1$, (c)$\Delta\epsilon = 2$, (d)$\Delta\epsilon = 4$

Fig.6 SEM micrographs of nickel taken in radial direction for $\epsilon_{eq,tot} = 64$ at (a) $\Delta\epsilon = 0.5$, (b)$\Delta\epsilon = 1$, (c)$\Delta\epsilon = 2$, (d)$\Delta\epsilon = 4$, (e) monotonically deformed

Fig.7 SEM micrographs of nickel deformed by HPT in radial direction for (a) $\epsilon_{eq} = 0.5$, (b) $\epsilon_{eq} = 1$, (c) $\epsilon_{eq} = 2$ and (d) $\epsilon_{eq} = 4$

Fig.8 Orientation maps of nickel in axial direction and the standard triangle, (a)$\Delta\epsilon = 0.5$;$\epsilon_{eq,tot} = 4$, (b)$\Delta\epsilon = 0.5$; $\epsilon_{eq,tot} = 16$, (c)$\Delta\epsilon = 0.5$;$\epsilon_{eq,tot} = 64$, (d)$\Delta\epsilon = 4$;$\epsilon_{eq,tot} = 4$, (e)$\Delta\epsilon = 4$; $\epsilon_{eq,tot} = 16$, (f)$\Delta\epsilon = 4$;$\epsilon_{eq,tot} = 64$, (g) $\epsilon_{eq,tot} = 64$, monotonically deformed

Fig.9 (a) Size of the structural elements of nickel as a function of the total equivalent strain (b) ratio between the length of the HAB and the LAB

Fig.10 Distribution of the missorientation angle in deformed nickel samples (a) Samples deformed with $\Delta\epsilon = 0.5$ and monotonically deformed sample, $\epsilon_{eq} = 64$ (b) Samples deformed with $\Delta\epsilon = 4$

Fig.11 (a) Cyclic stress strain curve in fatigued polycrystalline copper [38], (b) Cyclic torque strain curve and the monoton flow curve for iron, (c) Cyclic torque strain curve and the monoton flow curve for nickel ($\Delta\epsilon$,ϵ at $r = 3mm$)

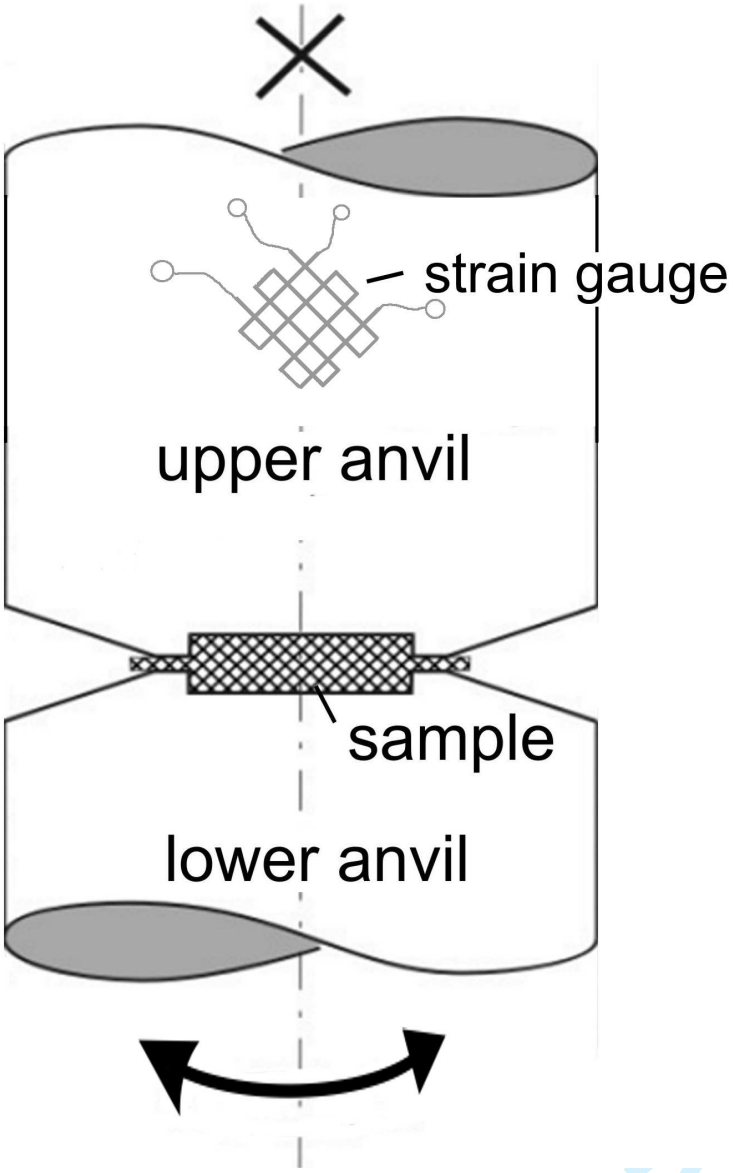
strain gauge
upper anvil
sample
lower anvil

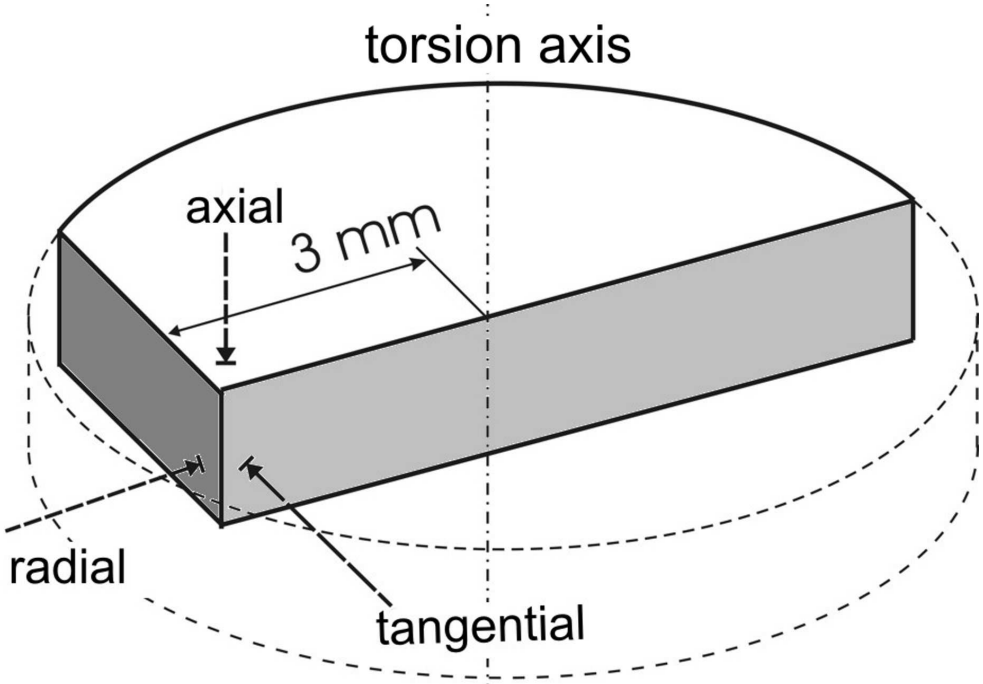

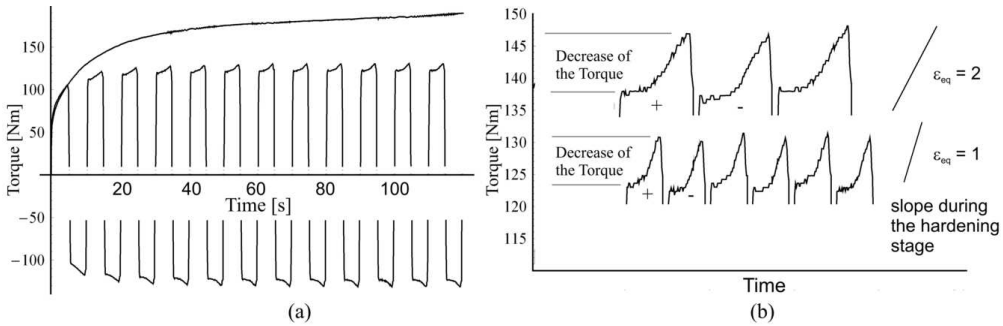

56x17mm (600 x 600 DPI)

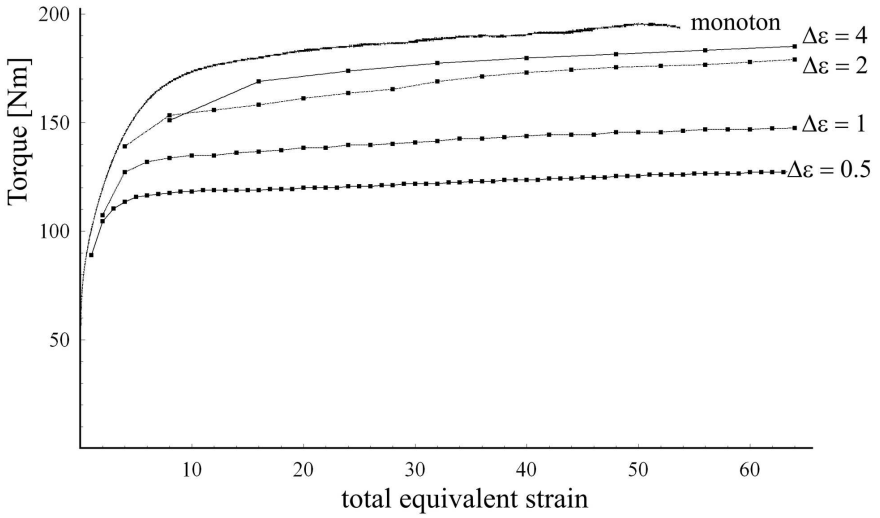

(a)

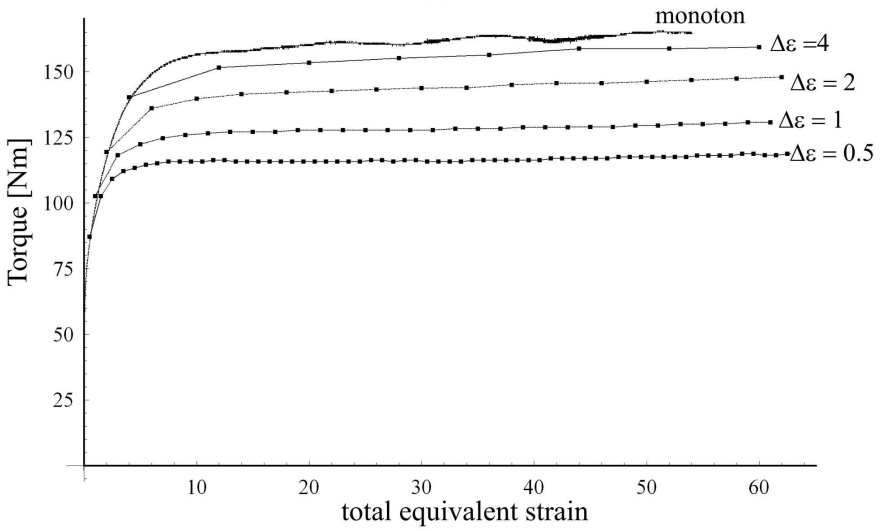

(b)

85x113mm (600 x 600 DPI)

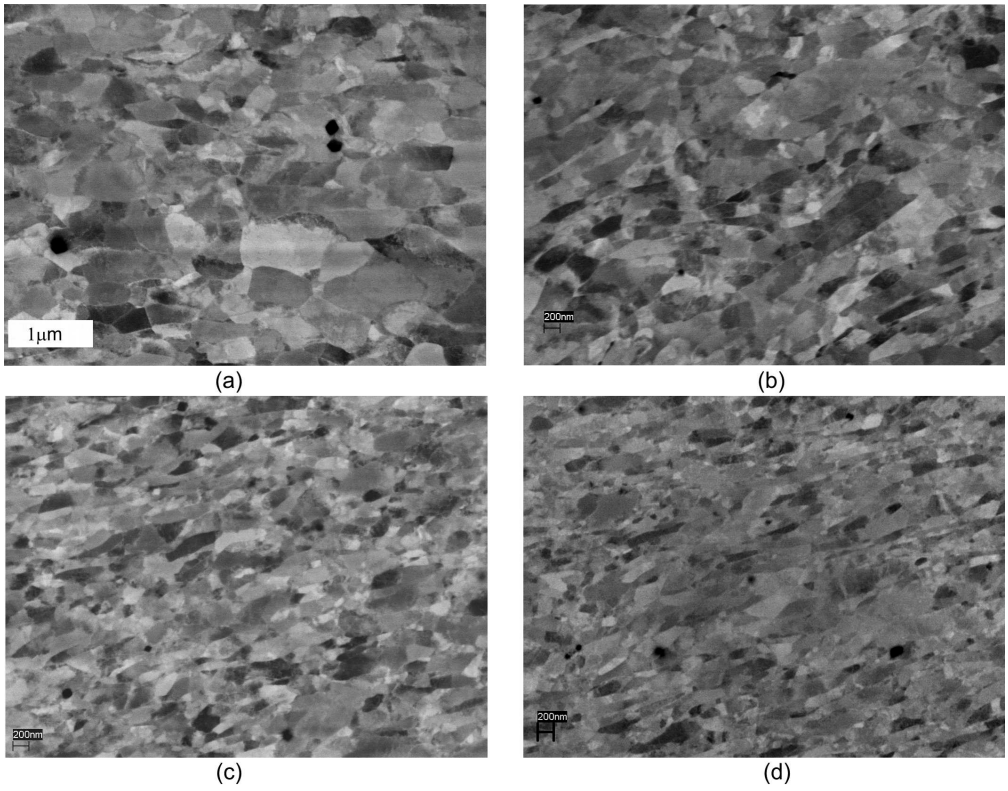

174x136mm (309 x 309 DPI)

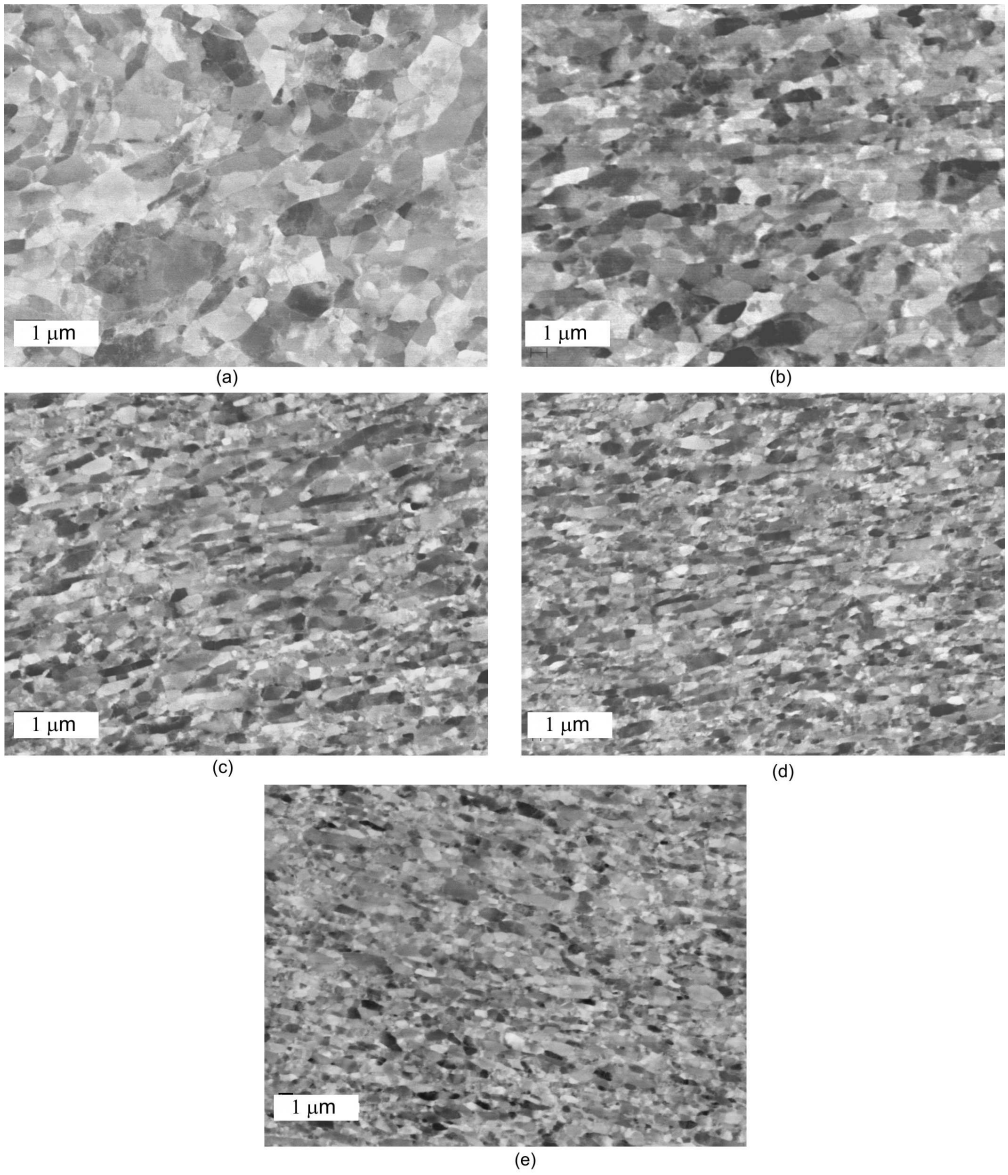

174x204mm (310 x 310 DPI)

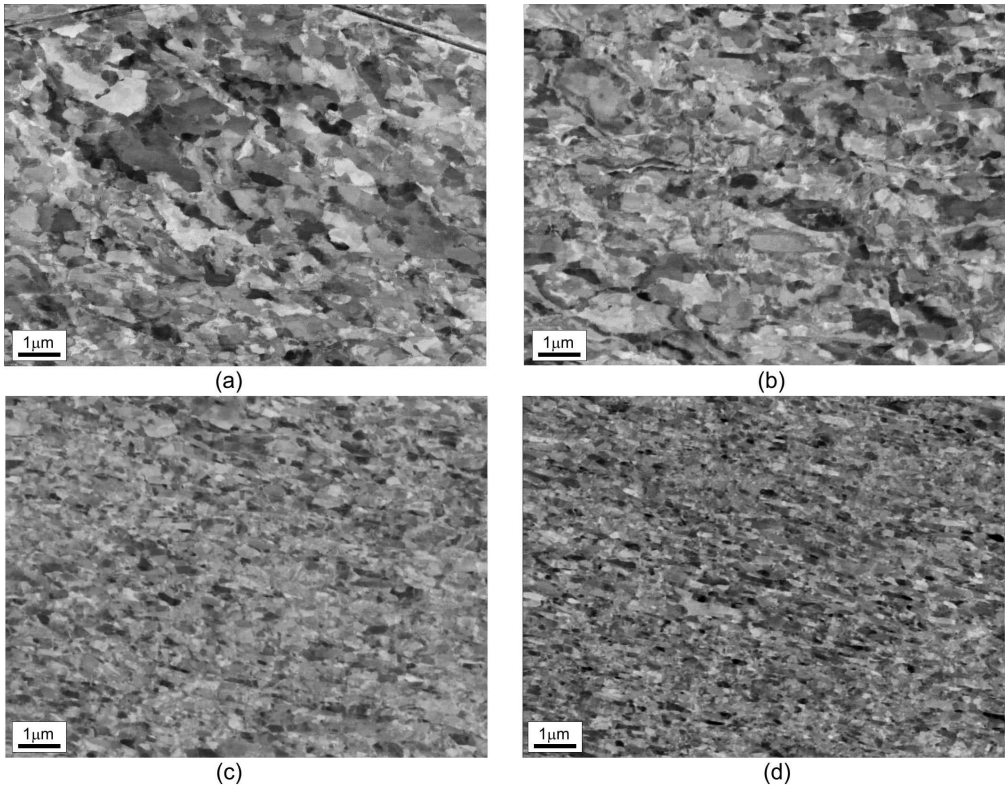

174x136mm (309 x 309 DPI)

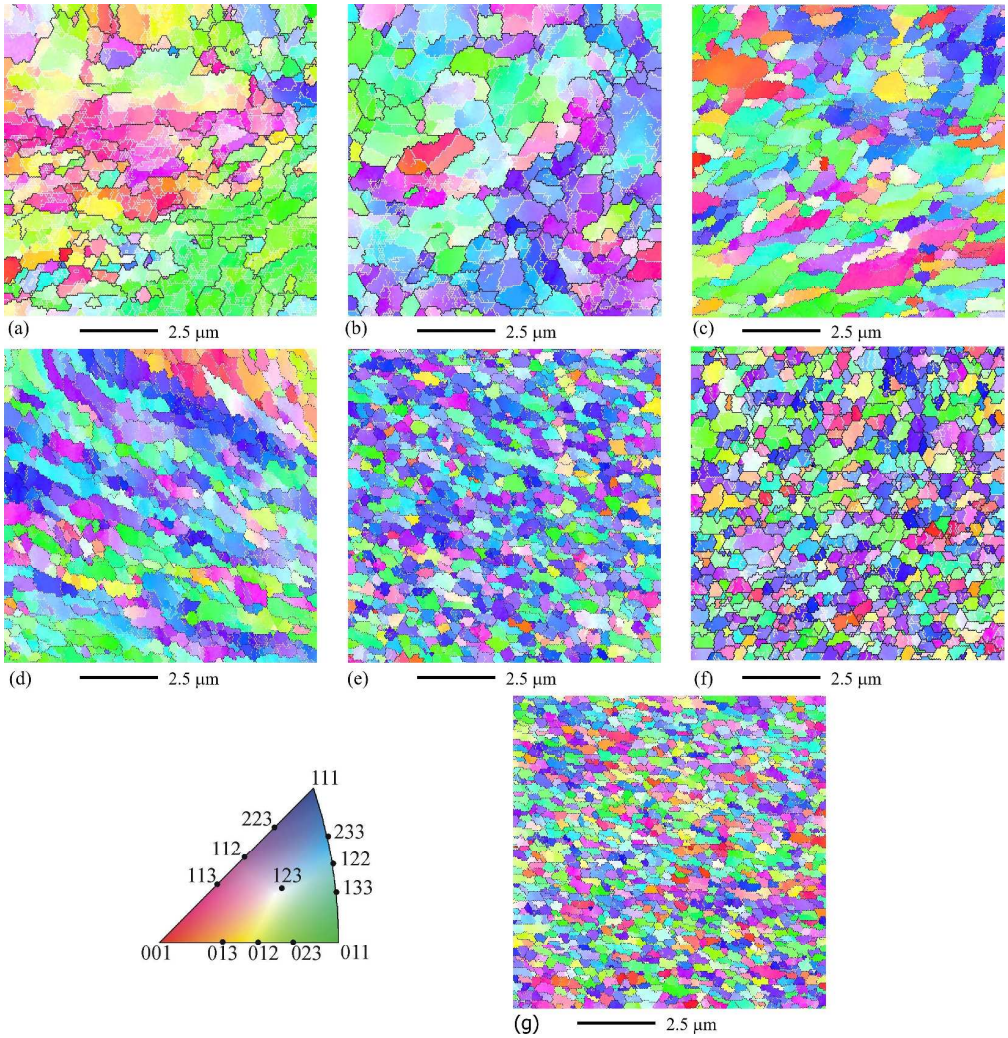

174x180mm (476 x 476 DPI)

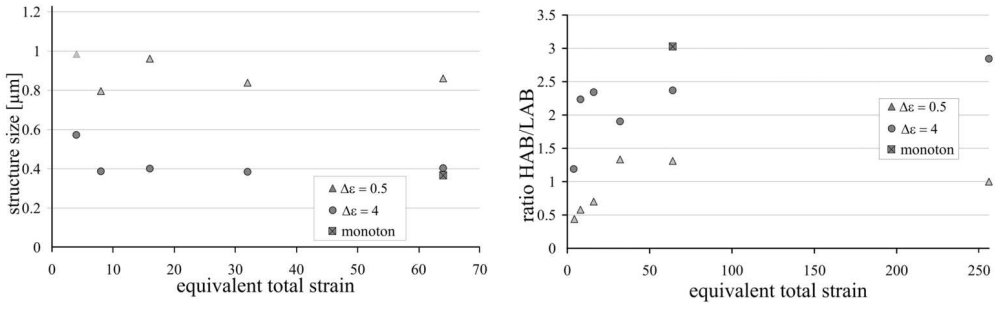

65x24mm (600 x 600 DPI)

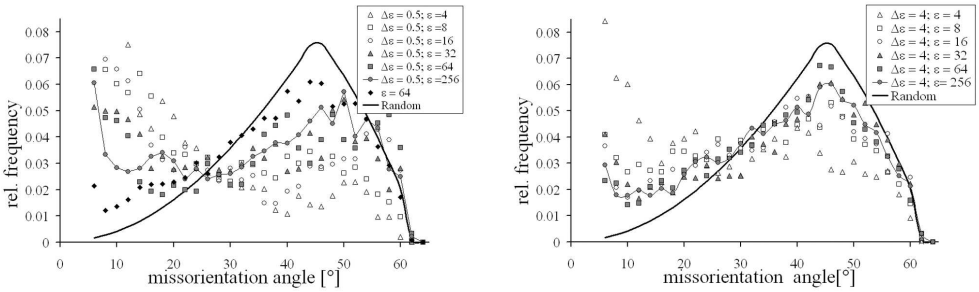

175x59mm (600 x 600 DPI)

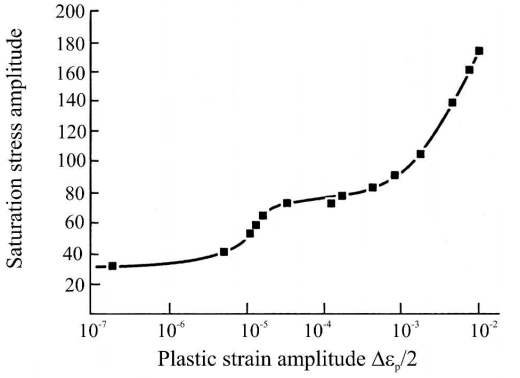

(a)

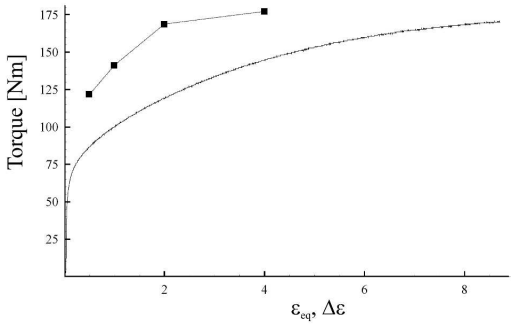

(b)

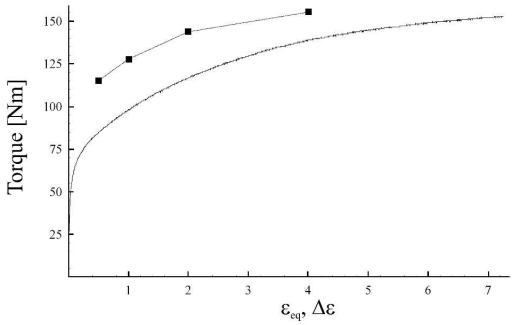

(c)

85x190mm (600 x 600 DPI)